Available online at www.sciencedirect.com
ScienceDirect
Trans. Nonferrous Met. Soc. China 22(2012) 2049−2056
Transactions of Nonferrous Metals Society of China
www.tnmsc.cn

# Enhanced photocatalytic properties of hierarchical nanostructured $TiO_2$ spheres synthesized with titanium powders

TAO Jie[1], DENG Jie[1], DONG Xiang[2], ZHU Hong[1], TAO Hai-jun[1]

1. College of Material Science and Technology, Nanjing University of Aeronautics and Astronautics, Nanjing 210016, China;
2. Faculty of Material Science and Engineering, Kunming University of Science and Technology, Kunming 650093, China

Received 4 July 2011; accepted 20 April 2012

**Abstract:** Using Ti powder as reagent, $TiO_2$ nanoneedle/nanoribbon spheres were prepared via hydrothermal method in NaOH solution. The samples were characterized by field emission scanning electron microscopy (FESEM), transmission electron microscopy (TEM) with selected area electron diffraction (SAED), X-ray diffraction (XRD), and UV-visible light absorption spectrum. The results indicate that the growth orientations of the crystals are influenced by the hydrothermal temperature and NaOH concentration. The diameter of the nanoneedle spheres and nanoribbon spheres (40−50 μm) are almost the same as that of Ti powders. $TiO_2$ nanoneedle/nanoribbon sphere powders are anatase after heat treatment at 450 °C for 1 h. Furthermore, methyl orange was used as a target molecule to estimate the photocatalytic activity of the specimens. Under the same testing conditions, the photocatalytic activities of the products decrease in the following order: $TiO_2$ nanoneedle sphere, $TiO_2$ nanoribbon sphere and P25.
**Key words:** nano-$TiO_2$; microsphere; photocatalytic properties; hydrothermal synthesis; Ti powders

## 1 Introduction

Nanostructural $TiO_2$ has recently attracted much attention in the fields of catalysis, adsorption, solar cells, electrochromic device, sensors and so on [1−4] because of its large surface area and enough active sites. However, the nature of easy agglomeration and hard recovery restricts the applications of nanoparticles. Compared with the immobilized nano-$TiO_2$, the hierarchical $TiO_2$ microspheres composed of the tailored nano-units combine the high reactivity of nano-materials and the easy recovery of micro-powders, thus becoming the researching hotspot [5−8].

The $TiO_2$ spheres are traditionally prepared from titanium halides or titanium alkoxides in the presence of hard/soft templates [5,9,10]. The used precursors are expensive, and the extra procedures including the preparation and the removal of templates complicate the $TiO_2$ synthesizing process and also increase the cost. $TiO_2$ spheres have also been fabricated using titanium halides [11−13] or Ti foils [14,15] as precursors without templates. An Ostwald ripening mechanism has been proposed for the spheres synthesized without templates [16,17].

Recently, three-dimensional (3D) flower-like $TiO_2$ nanostructures composed of many thin nanoribbons were synthesized through a hydrothermal reaction between NaOH solution and the mixture of Ti powders, $H_2O_2$ and $HNO_3$ [18,19]. In this work, a simple reaction system just including NaOH solution and Ti powders is first used to hydrothermally synthesize $TiO_2$ nanoneedle/nanoribbon microsphere powders. The morphologies of the as-prepared $TiO_2$ microsphere powders are quite different from the one-dimensional (1D) nanostructures which always occur in the hydrothermal treatment of Ti foils and NaOH solution [20−22]. This study provides a new synthesis method of controllable $TiO_2$ nanostructures by tuning the morphologies of raw materials and the hydrothermal conditions. The morphologies, structures, and photocatalytic properties of the microsphere are characterized. A possible

**Foundation item:** Project (NS2010153) supported by Nanjing University of Aeronautics and Astronautics Research Funding, China; Project (BE2009130) supported by Jiangsu Key Technology R&D Program, China
**Corresponding author:** TAO Jie; Tel: +86-25-84895378; Fax: +86-25-52112626; E-mail: taojie@nuaa.edu.cn
DOI: 10.1016/S1003-6326(11)61427-1

mechanism is also proposed. Finally, the photocatalytic activities of the products are studied.

## 2 Experimental

The titanium powders (99.9% purity) with a diameter of 40−50 μm were ultrasonically cleaned in acetone and ethanol for 30 min respectively, and then dried in an oven before use. In order to synthesize nanoneedle spheres, 0.2 g Ti powders were put into a 100 mL Teflon-lined stainless steel autoclave with 70 mL of 5 mol/L NaOH solution. The autoclave was heated to 210 °C for 48 h in the oven. After the hydrothermal treatment, the specimen was completely washed with 0.1 mol/L HCl solution and distilled water respectively for several times. Finally, the sample was dried in the oven, and sintered at 450 °C for 1 h. The process for preparing nanoribbon spheres was almost the same as that of nanoneedle spheres except that the concentration of NaOH solution was 7 mol/L and the hydrothermal temperature was 180 °C.

The morphologies of the samples were analyzed by field emission scanning electron microscope (FESEM) (LEO−1530VP) and transmission electron microscope (TEM) (FEI Tecnai $G^2$) with selected area electron diffraction (SAED). The X-ray diffraction (XRD) measurement was performed with a Bruker D8 diffractometer. The UV-visible light absorption spectra of the as-prepared specimens were detected using Cary 100 UV-visible spectrophotometer with a DAR-CA-30I integrating sphere.

$TiO_2$ photocatalysts were irradiated under UV light to decompose the adsorbed pollutants. The aqueous system containing 50 mL of 20 mg/L methyl orange (MO) and 0.1 g as-synthesized $TiO_2$ photocatalysts was magnetically stirring in dark for 1 h to reach the adsorption equilibrium of MO with the photocatalysts, and then exposed to UV light from a high pressure mercury lamp (250 W). The distance between the aqueous system and the light source was 15 cm. Commercial $TiO_2$, Degussa P25, was adopted as the reference to assess the photocatalytic activity of $TiO_2$ spheres under the same experimental conditions. The concentration of MO left in the aqueous system was measured at different time intervals by detecting the absorption at 463.5 nm on a UV-visible spectrophotometer (Cary 100).

## 3 Results and discussion

The Ti powders were treated in the NaOH solution with lower concentration (5 mol/L). The morphologies of the specimens are presented in Figs. 1(a) and (b). It can be seen that the products are nanoneedle spheres with a diameter of 40−50 μm, which is the same as the diameter of Ti powder. The diameter and length of the nanoneedle spheres are ~200 nm and ~20 μm respectively. As shown in Figs. 1(a) and (b), the nanoneedle spheres are composed of nanoneedles without any Ti powders left. Therefore, it can be deduced that Ti powders have

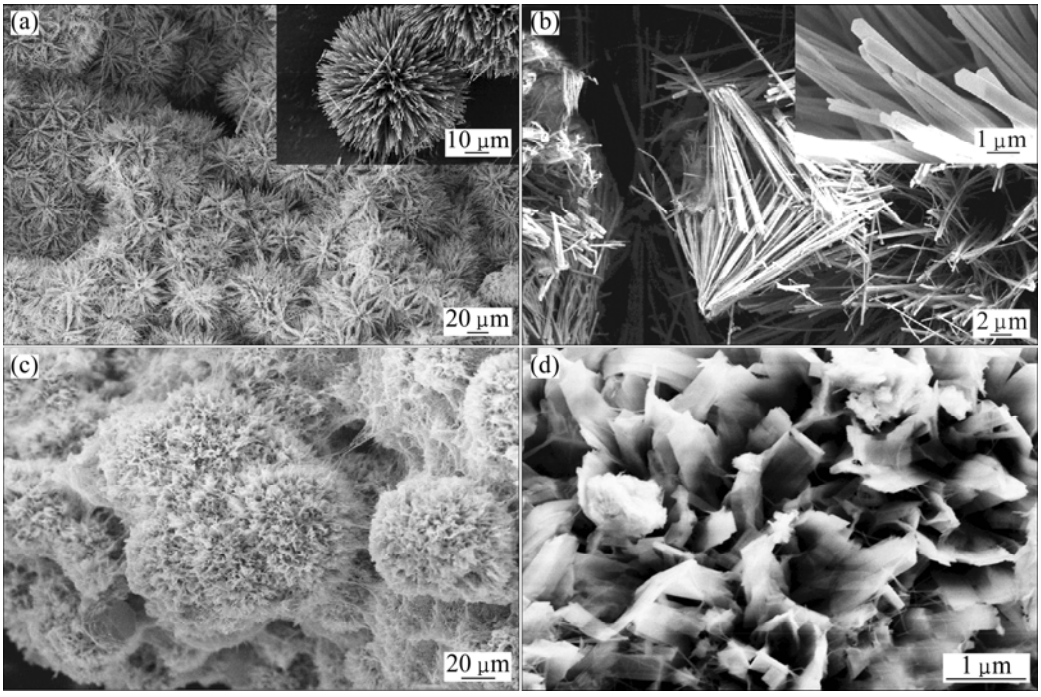


**Fig. 1** FESEM images of $TiO_2$ nanoneedle spheres (a, b) (inset is higher-magnification) and nanoribbon spheres (c, d)

completely reacted with NaOH under this hydrothermal condition. The FESEM images of the samples prepared in 7 mol/L NaOH solution at 180 °C for 48 h (Figs. 1(c) and (d)) show that the products are nanoribbon spheres with a diameter of 40−50 μm, also the same as Ti powders. The thickness and width of the nanoribbon are ~30 nm and ~200 nm respectively. As shown in Fig. 1, both the nanoneedle and nanoribbon are all radial alignment, which proves that the titanate crystals grow along the radial direction of the Ti particle. Based on the above observations, it can be concluded that the morphology and structure of the products are mainly influenced by hydrothermal temperature and solution concentration. The appropriate solution concentration and proper hydrothermal temperature can make the titanate crystals grow along the radial direction of the Ti particle.

Figure 2 shows the TEM results of segments of the nanoneedle sphere and nanoribbon sphere. The TEM image (Fig. 2(a)) demonstrates that the diameter and length of the nanoneedle are ~200 nm and ~20 μm respectively, which are in accordance with the results of FESEM images. The SAED image of the nanoneedles was not obtained because the electron beam can not penetrate the thicker nanoneedles. The SAED image of Fig. 2(b) shows that the nanoribbons are well crystalline. Based on the FESEM and TEM observations of the specimens, it can be proposed that there are no Ti powders left in the samples after the hydrothermal treatment. In fact, the XRD results corroborated this conclusion.

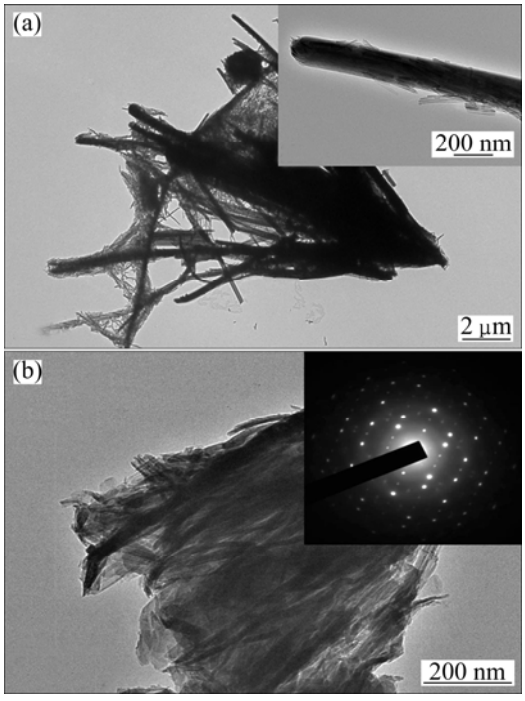


**Fig. 2** TEM images of segments of $TiO_2$ nanoneedle spheres (inset is higher-magnification) (a) and nanoribbon spheres (inset is its SAED pattern) (b)

The powder XRD patterns of the two samples are shown in Fig. 3. Both of the synthesized powders display a good crystallinity. The XRD patterns of the samples match well with the anatase phase, which can be assigned to the (101), (004), (200), (105), (211), (204) planes of anatase $TiO_2$ (JCPDS 21−1272). Meanwhile, no characterized peaks of pure Ti can be observed in Fig. 3. The XRD results indicate that the crystallographic phases of all the specimens sintered at 450 °C for 1 h belong to tetragonal anatase $TiO_2$.

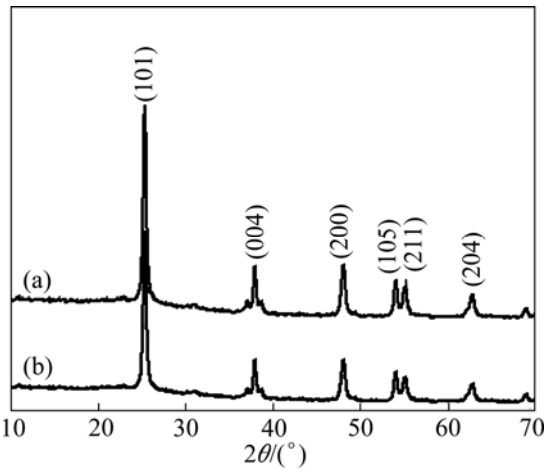


**Fig. 3** XRD patterns of $TiO_2$ nanoneedle spheres (a) and nanoribbon spheres (b)

The effects of hydrothermal conditions on the morphologies of the film were further discussed. FESEM images of nanomaterials synthesized in a 3 mol/L NaOH solution at 180 °C for different reaction time are presented in Fig. 4. The lower concentration (3 mol/L) and appropriate temperature (180 °C) are chosen so that the whole growth process can be observed. As shown in Figs. 4(a) and (b), smaller spheres with a diameter of less than 10 μm are formed on the surface of Ti particles when the reaction time is 12 h. These spheres connect together and are composed of nanowires and nanoplates. The diameter of the connected spheres formed on the surface of Ti particles remains to be about 10 μm when the reaction time is extended to 24 h (Figs. 4(c) and (d)), while the nanowires reduce and the spheres are mainly composed of nanoplates compared with Fig. 4(b). The nanowires disappear and the nanoplates break up into nanoribbons when the time further increases to 48 h (Figs. 4(e) and (f)). The diameter of the spheres becomes larger than 10 μm and the spheres are completely composed of nanoribbons. The narrower nanobelts come into being because of the shrinkage of the nanoribbons

when the reaction time is 72 h, as shown in Figs. 4(g) and (h). It can be inferred from the results that 1D nano-units would form by prolonging the reaction time.

Figure 5 shows SEM images of nanomaterials synthesized in different NaOH concentrations at 210 °C for 48 h. As shown in Figs. 5(a) and (b), narrow nanobelt microspheres form in 3 mol/L NaOH solution. When 7 mol/L NaOH solution is used, the mixture of long nanowires and nanorods takes shape. The results show that the $TiO_2$ morphology experiences nanobelt spheres, nanoneedle spheres and nanowires when the concentration of NaOH solution changes from 3 and 5 to 7 mol/L.

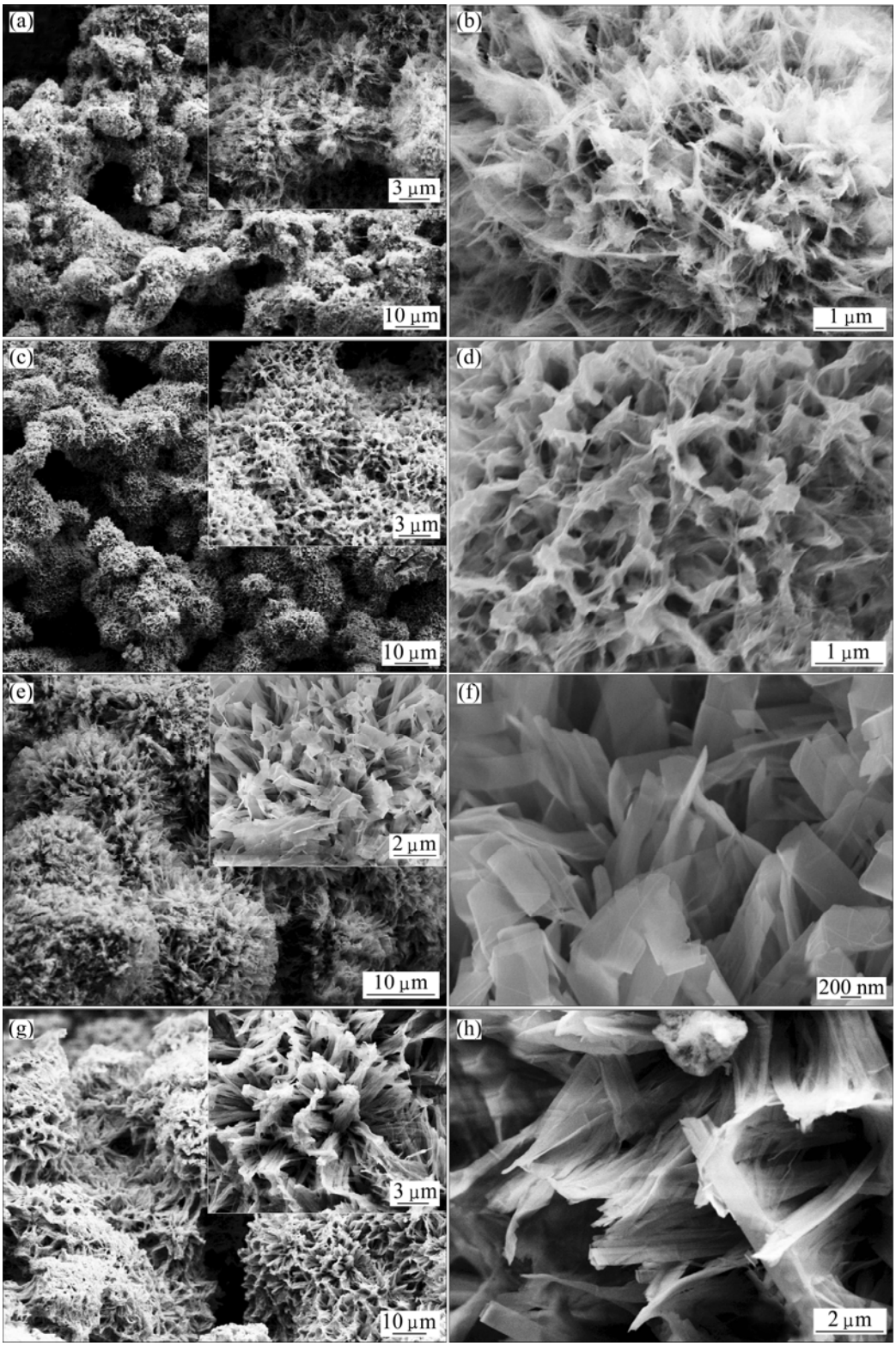


**Fig. 4** FESEM images of samples synthesized in 3 mol/L NaOH solution at 180 °C: (a, b) 12 h; (c, d) 24 h; (e, f) 48 h; (g, h) 72 h (inset is higher-magnification)

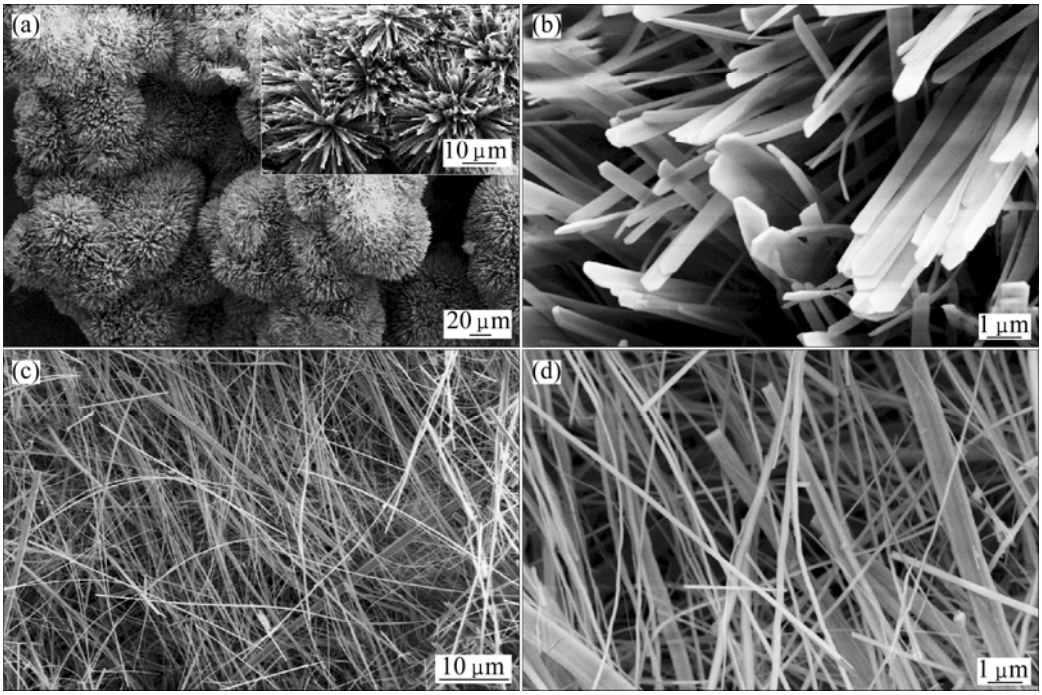


**Fig. 5** FESEM images of samples synthesized in 3 mol/L (a, b), and 7 mol/L (c, d) NaOH solution at 210 °C for 48 h (inset is higher-magnification)

From the above results, it can be concluded that the hydrothermal conditions have great influence on the morphology of the sample. Prolonging the reaction time, increasing NaOH concentration and raising the temperature (comparing the images of samples synthesized in 3 mol/L NaOH at 180 °C or 210 °C and 7 mol/L NaOH at 180 °C or 210 °C), all favor the decrease of $TiO_2$ nanostructural dimension from 2D nanoplates/ nanoribbons/nanobelts to 1D nanoneedles/nanorods/ nanowires.

According to the former reports [15,23], the dissolution−growth mechanism is proposed as the possible formation mechanism of the spheres. In the beginning, the Ti particles react with NaOH solution and many titanate nano-crystals are created and cover on the surface of Ti particles [22]. Then, these nano-crystals transform into a nucleus, from which the one dimensional nano-titanates begin to grow. The growth of nano-titanates in the cross direction is inhibited because of the competitive growth from too many nuclei simultaneously, whereas the growth in the direction perpendicular to the Ti particles substrate is free. As a result, one dimensional nano-titanates begin to grow along the radial direction of Ti particles through a dissolution−growth (recrystallization) process [22,24]. It is noticed that the morphologies and structures of the products are drastically affected by the hydrothermal temperature and solution concentration. Both low concentration NaOH solution and low temperature slow down the Ti oxidation rate, resulting in lower concentration of Ti precursor in the growth solution. In the other hand, high temperature and high concentration of NaOH solution both increase the Ti oxidation rate and thus raise the concentration of Ti precursor, leading to increasing the growth rate of titanate crystals in the cross direction. Then, high temperature with low solution concentration or low temperature with high solution concentration would guarantee the titanate crystals grow along the radial direction of the Ti particles, and structures would be varied ( nanoneedle spheres: 210 °C, 5 mol/L; nanoribbon spheres: 180 °C, 7 mol/L).

Figure 6 shows the UV-visible absorption spectra of the samples. The $TiO_2$ nanoneedle spheres exhibit stronger adsorption than the $TiO_2$ nanoribbon spheres in the UV-vis range of 300−700 nm. It has been reported that the $TiO_2$ microspheres present superior light scattering ability, which can increase its light absorption [9,11,15]. In this work, though $TiO_2$ nanoribbon spheres can scatter the incident light as a result of spherical structure, the nanoribbons (~30 nm) are so thin that the incident light can transmit the nanoribbon, thus weakening the light scattering ability of the $TiO_2$ nanoribbon spheres.

The photocatalytic activities of the synthesized $TiO_2$ nanostructures were tested with methyl orange (MO) as a model pollutant and Degussa P25 as the reference. Figure 7 shows the changes in the concentration of MO under UV illumination in the presence of different $TiO_2$

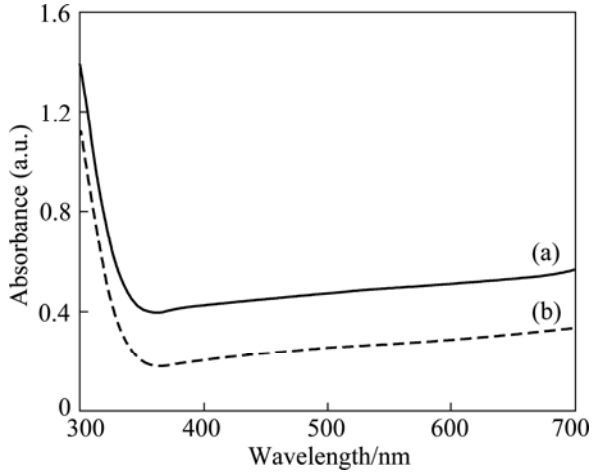


**Fig. 6** UV-visible absorption spectra of $TiO_2$ nanoneedle spheres (a) and nanoribbon spheres (b)

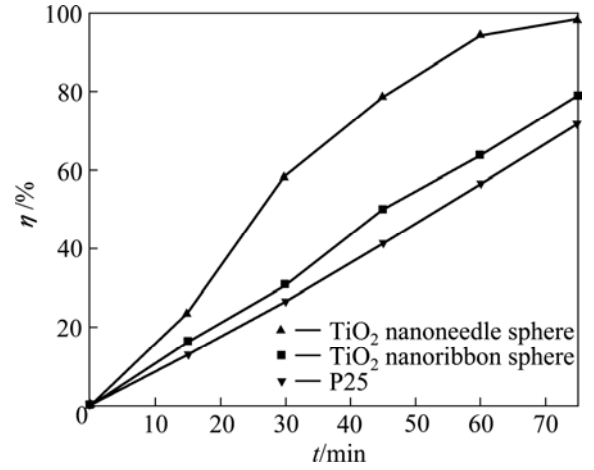


**Fig. 7** Photocatalytic degradation efficiencies of MO in aqueous solution with three photocatalysts

nanostructures by recording the UV-visible spectra at 15 min interval. The photocatalytic activities of the tested samples increase in the following order: P25 < $TiO_2$ nanoribbon spheres < $TiO_2$ nanoneedle spheres. The unique nanostructure of the $TiO_2$ nanoneedle spheres is also contributed to its highest photocatalytic ability among all samples. The enhancement of the effect derived from the special hierarchical structure of the $TiO_2$ nanoneedle spheres includes three aspects. Firstly, one-dimensional nanoneedles can provide conventional channels for fast electron transfer, thus decreasing the photo-generated carriers' recombination and increasing their utilization efficiencies. Secondly, the hierarchical $TiO_2$ nanostructural microspheres still maintain the larger surface area of nano-materials which comes from the less agglomeration of microspheres, thus having the higher reactivity compared with P25 nanoparticles. Finally, the increased light-harvesting ability of the $TiO_2$ nanoneedle spheres which derives from the light scattering is helpful for its photocatalytic activity. The light will be multiplely absorbed during the transporting process, leading to the improvement of the light harvesting abilities of the $TiO_2$ nanoneedle spheres. Spontaneously, the more photons are absorbed, and the more photo-carriers are produced, resulting in the higher photocatalytic ability. $TiO_2$ nanoribbon spheres can also provide direct transferring pathway for photo-generated electrons. Whereas, the light scattering ability of the $TiO_2$ nanoribbon spheres is lower than that of $TiO_2$ nanoneedle spheres. Therefore, the lower light harvesting ability induces the lower photocatalytic abilities. P25 is just a kind of $TiO_2$ nanoparticles which cannot enhance the light harvesting [25] and the photo-generated carriers' utilization efficiencies, so the photocatalytic ability of P25 is the lowest among all samples.

The linear relationship of ln $A_0/A$ vs time (Fig. 8) shows the photocatalytic degradation of MO follows the pseudo-first-order kinetics:

$$\ln\frac{A_0}{A} = a + kt$$

where $A_0/A$ is the normalized MO concentration, $t$ is the reaction time, and $k$ is the apparent reaction rate in terms of $s^{-1}$. The apparent photochemical degradation rate constants of the $TiO_2$ nanoneedle spheres, $TiO_2$ nanoribbon spheres and P25 are $9.38\times10^{-4}$ $s^{-1}$, $3.33\times10^{-4}$ $s^{-1}$, and $2.75\times10^{-4}$ $s^{-1}$, respectively. It is further confirmed that the synthesized $TiO_2$ nanostructures possess advantages both in high photocatalytic efficiency and easy recycle, which will enlarge the application field of $TiO_2$ in the environmental treatment.

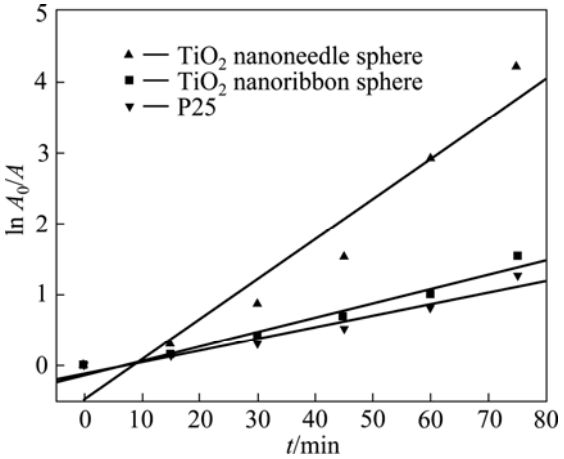


**Fig. 8** First-order kinetic rate plots for photochemical degradation of MO

## 4 Conclusions

1) The novel $TiO_2$ nanoneedle spheres and $TiO_2$ nanoribbon spheres were successfully prepared with Ti

powders by hydrothermal method. The diameter of the $TiO_2$ nanoneedle or nanoribbon spheres was between 40 and 50 μm, which is almost the same as that of Ti particles.

2) The $TiO_2$ nanoneedle spheres and $TiO_2$ nanoribbon spheres presented superior photocatalytic activities compared with the nano-particle $TiO_2$ (P25). The decreased recombination rate of the photo-generated electron-hole pair, the larger surface area and the enhanced light-harvesting ability were the key impacting factors for the superior photocatalytic characteristics of $TiO_2$ nanoneedle spheres and $TiO_2$ nanoribbon spheres.

3) As the outstanding photocatalytic characteristics, the synthesized $TiO_2$ nanostructures are promising candidate for environmental applications, possessing the advantages both in high photocatalytic efficiency and in easy recycle. Furthermore, the approach described here provides a low-cost method to largely synthesize the micro-size $TiO_2$ consisting of nanostructural units.

## References


[1] CHEN X B, MAO S S. Titanium dioxide nanomaterials: Synthesis, properties, modifications, and applications [J]. Chem Rev, 2007, 107: 2891−2959.

[2] YU J G, LIU S W, YU H G. Microstructures and photoactivity of mesoporous anatase hollow microspheres fabricated by fluoride-mediated self-transformation [J]. J Catal, 2007, 249: 59−66.

[3] ZHONG Z Y, YIN Y D, GATES B, XIA Y N. Preparation of mesoscale hollow spheres of $TiO_2$ and $SnO_2$ by templating against crystalline arrays of polystyrene beads [J]. Adv Mater, 2000, 12: 206−209.

[4] KOO H J, KIM Y J, LEE Y H, LEE W I, KIM K, PARK N. Nano-embossed hollow spherical $TiO_2$ as bifunctional material for high-efficiency dye-sensitized solar cells [J]. Adv Mater, 2008, 20: 195−199.

[5] BALA H, YU Y, ZHANG Y. Synthesis and photocatalytic oxidation properties of titania hollow spheres [J]. Mater Lett, 2008, 62: 2070−2073.

[6] KIM Y J, CHAI S Y, LEE W I. Control of $TiO_2$ structures from robust hollow microspheres to highly dispersible nanoparticles in a tetrabutylammonium hydroxide solution [J]. Langmuir, 2007, 23: 9567−9571.

[7] IKARI H, OKANISHI K, TOMITA M, ISHIDATE T. Fluorescence MDR features of $Eu^{3+}$ doped sol−gel $TiO_2$ hydrate microspheres [J]. Opt Mater, 2008, 30: 1323−1326.

[8] TSAI M C, TSAI T L, LIN C T, CHUNG R J, SHEU H S, CHIU HT, LEE C Y. Tailor made mie scattering color filters made by size-tunable titanium dioxide particles [J]. J Phys Chem C, 2008, 112: 2697−2702.

[9] PAN J H, ZHANG X W, DU A J, SUN D D, LECKIE J O. Self-etching reconstruction of hierarchically mesoporous F−$TiO_2$ hollow microspherical photocatalyst for concurrent membrane water purifications [J]. J Am Chem Soc, 2008, 130: 11256−11257.

[10] SHI H J, CHEN Q F, XU Y, LV B L, WU D. PMMA-templated synthesis of porous $TiO_2$ micro-spheres and application in photocatalysis [J]. Acta Chim Sinica, 2011, 69(8): 863−869. (in Chinese)

[11] ZHOU J K, LV L, YU J, LI H L, GUO P Z, SUN H, ZHAO X S. Synthesis of self-organized polycrystalline F-doped $TiO_2$ hollow microspheres and their photocatalytic activity under visible light [J]. J Phys Chem C, 2008, 112(14): 5316−5321.

[12] GUO C, GE M, LIU L, GAO G, FENG Y, WANG Y. Directed synthesis of mesoporous $TiO_2$ microspheres: Catalysts and their photocatalysis for bisphenol A degradation [J]. Environ Sci Technol, 2010, 44(1): 419−425.

[13] SHANG S, JIAO X, CHEN D. Template-free fabrication of $TiO_2$ hollow spheres and their photocatalytic properties [J]. ACS Appl Mater Inter, 2012, 4(2): 860−865.

[14] DONG X, TAO J, LI Y, ZHU H. Enhanced photoelectrochemical properties of F-containing $TiO_2$ sphere thin film induced by its novel hierarchical structure [J]. Appl Surf Sci, 2009, 255: 7183−7187.

[15] WU G, WANG J, THOMAS D F, CHEN A. Synthesis of F-doped flower-like $TiO_2$ nanostructures with high photoelectrochemical activity [J]. Langmuir, 2008, 24(7): 3503−3509.

[16] LI J, ZENG H. Hollowing Sn-doped $TiO_2$ nanospheres via Ostwald ripening [J]. J Am Chem Soc, 2007, 129: 15839−15847.

[17] LIU Z Y, SUN D D, GUO P, LECKIE J O. One-step fabrication and high photocatalytic activity of porous $TiO_2$ hollow aggregates by using a low-temperature hydrothermal method without templates [J]. Chem Eur J, 2007, 13(6): 1851−1855.

[18] LIU M, LU W, ZHAO L, ZHOU C, LI H, WANG W. Fabrication and photocatalytical properties of flower-like $TiO_2$ nanostructures [J]. Transactions of Nonferrous Metals Society of China, 2010, 20: 2299−2302.

[19] LIU M, PIAO L, WANG W. Fabrication and characteristics of three-dimensional flower-like titanate nanostructures [J]. J Nanosci and Nanotechno, 2010, 10(11): 7469−7472.

[20] PENG X, CHEN A. Large-scale synthesis and characterization of $TiO_2$-based nanostructures on Ti substrates [J]. Adv Funct Mater, 2006, 16: 1355−1362.

[21] GUO Y, LEE N, OH H, YOON C, PARK K, LEE W, LI Y, LEE H, LEE K, KIM S. Preparation of titanate nanotube thin film using hydrothermal method [J]. Thin Solid Films, 2008, 516: 8363−8371.

[22] WANG W, LIN H, JI J, WANG N. Formation of titania nanoarrays by hydrothermal reaction and their application in photovoltaic cells [J]. J Am Ceram Soc, 2008, 91(2): 628−631.

[23] HU X, ZHANG T, JIN Z, HUANG S, FANG M, WU Y, ZHANG L. Single-crystalline anatase $TiO_2$ dous assembled micro-sphere and their photocatalytic activity [J]. Cryst Growth Des, 2009, 9(5): 2324−2328.

[24] LIU B, BOERCKER J E, AYDIL E S. Oriented single crystalline titanium dioxide nanowires [J]. Nanotechnology, 2008, 19: 505604−505610.

[25] DONG X, TAO J, LI Y Y, WANG T, ZHU H. Photoelectrochemical properties of three-dimensional network $TiO_2$ nanowire film prepared by hydrothermal method [J]. Acta Phys-Chim Sin, 2009, 25(9): 1874−1882. (in Chinese)

# 钛粉制备多级纳米结构 $TiO_2$ 微球及其光催化特性

陶　杰[1]，邓　杰[1]，董　祥[2]，朱　宏[1]，陶海军[1]

1. 南京航空航天大学 材料科学与技术学院，南京 210016；
2. 昆明理工大学 材料科学与工程学院，昆明 650093

**摘　要**：在 NaOH 溶液中采用水热法处理钛粉制备 $TiO_2$ 纳米针/带微球。利用场发射扫描电子显微镜(FESEM)、透射电子显微镜(TEM)、选区衍射(SAED)、紫外−可见吸收光谱(UV-vis)和 X 射线衍射仪(XRD)对样品结构进行表征。结果显示，水热温度和溶液浓度共同决定晶体的生长方向，纳米针/带微球的直径(40~50 μm)与钛粉直径相当。纳米针/带微球经 450 °C 热处理 1 h 后转变锐钛矿。以甲基橙为目标考察样品的光催化活性。在相同条件下，样品的光催化活性为：$TiO_2$ 纳米针微球> $TiO_2$ 纳米带微球> P25。

**关键词**：纳米 $TiO_2$；微球；光催化性能；水热制备；钛粉

**(Edited by YUAN Sai-qian)**